

# Equilibration of Topological Defects at the Deconfined Quantum Critical Point

Yu-Rong Shu,<sup>1</sup> Shao-Kai Jian,<sup>2</sup> Anders W. Sandvik,<sup>3,\*</sup> and Shuai Yin<sup>4,†</sup>

<sup>1</sup>*School of Physics and Electronic Engineering, Guangzhou University, Guangzhou 510006, China*

<sup>2</sup>*Department of Physics and Engineering Physics,  
Tulane University, New Orleans, Louisiana, 70118, USA*

<sup>3</sup>*Department of Physics, Boston University, Boston, Massachusetts 02215, USA*

<sup>4</sup>*School of Physics, Sun Yat-Sen University, Guangzhou 510275, China*

(Dated: May 9, 2023)

Deconfined quantum criticality (DQC) arises from fractionalization of quasi-particles and leads to fascinating behaviors beyond the Landau-Ginzburg-Wilson (LGW) description of phase transitions. The unusual aspects of DQC in equilibrium also suggest exotic phenomena out of equilibrium, which are still largely unexplored. Here we study manifestations of DQC when driving (quantum annealing) a two-dimensional quantum magnet through a critical point separating antiferromagnetic and spontaneously dimerized ground states. Numerical simulations show that the celebrated Kibble-Zurek scaling (KZS) mechanism is inadequate for describing the annealing process. To explain our results, we introduce the concept of dual asymmetric KZS, where a deconfinement time enters in addition to the conventional relaxation time and the scaling also depends on the direction in which the system is driven through the critical point according to a duality principle connecting the topological defects in the two phases. These defects—spinons in the dimerized phase and space-time hedgehogs in the antiferromagnetic phase—require a much longer time scale for equilibration than the amplitude of the order parameter. Beyond the new insights into DQC, our scaling approach provides a new window into out-of-equilibrium criticality with multiple length and time scales.

The concept of deconfined quantum criticality (DQC) was introduced [1–3] as a paradigm beyond that of Landau-Ginzburg-Wilson (LGW) for certain continuous phase transitions between ordered ground states with unrelated broken symmetries. Though evidence for critical points with fractionalized excitations and emergent gauge fields has been found in simulations of lattice models [4–12], the exact nature of the DQC phenomenon is still under intense scrutiny [13–22].

In the paradigmatic example of DQC between the antiferromagnetic (AFM) and spontaneously dimerized valence-bond-solid (VBS) phases of spin-isotropic  $S = 1/2$  magnets on the two-dimensional (2D) square lattice, the quantum numbers carried by topological defects in one phase correspond to the order parameter in the other phase. Specifically, the theory posits that fractionalized spin excitations (spinons) in the VBS phase and space-time hedgehog singularities (monopoles) in the AFM phase deconfine upon approaching the critical point and proliferate when crossing the phase transition, thereby inducing the complementary order parameter. Quantum interference between Berry phases of monopoles makes their fugacity irrelevant at the critical point [1, 2]. The associated emergent U(1) symmetry of the near-critical VBS phase (where quadrupled monopoles are “dangerously” irrelevant) was confirmed [4, 6], and a higher SO(5) symmetry at the critical point in one variant of the theory [3] has also been detected [10, 23]. In addition to the conventional correlation length  $\xi$ , a more strongly divergent confinement length scale  $\xi'$  should exist; it has

been characterized in simulations including spinon pairs in the VBS phase [11, 24].

Universal critical phenomena are manifested not only in equilibrium states but also in nonequilibrium processes. We here study dynamical aspects of DQC through quantum annealing of a 2D spin model, uncovering novel scaling behaviors stemming from slow equilibration of topological defects at the AFM–VBS transition.

Within the conventional LGW description, when tuning a parameter  $g = \pm v|t|$  (a reduced temperature or some parameter of the Hamiltonian) versus time  $t$ , such that  $g = 0$  is a classical or quantum critical point, the velocity ( $v$ ) dependence of the correlation length and other critical properties are described by the Kibble-Zurek scaling (KZS) mechanism [25–28], which we outline first.

During the initial stage of an annealing process, the temporal distance  $|t|$  to the critical point should exceed the relaxation time  $\zeta \propto \xi^z$  ( $z$  being the dynamic critical exponent). The system remains in equilibrium with correlation length  $\xi(t) \sim |g(t)|^{-\nu}$  until entering the impulse stage when  $|t| < \zeta(t)$ , falling out of equilibrium with the correlation length frozen at

$$\xi_v \sim v^{-1/r}, \quad r \equiv z + 1/\nu. \quad (1)$$

As a consequence, physical quantities are controlled by  $\xi_v$  instead of  $\xi$  from that point until  $g = 0$ .

More precisely, because of Eq. (1) the order parameter  $P$  for a system of size  $L$  satisfies an extended finite-size scaling form that can be written as [29–32]

$$P^2(v, L) = L^{-2\beta/\nu} f_P(vL^r, gL^{1/\nu}), \quad (2)$$

where  $\beta$  is the standard equilibrium critical exponent of  $P$ . The scaling function  $f_P$  depends on the direction of

\* sandvik@bu.edu

† yinsh6@mail.sysu.edu.cn

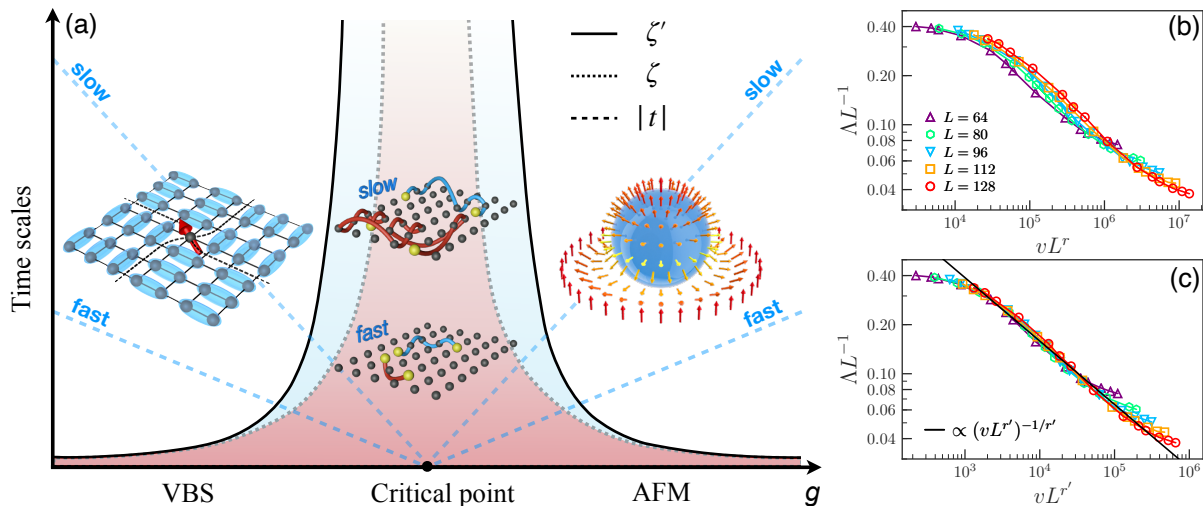


FIG. 1. **Topological defects and divergent time scales.** (a) Illustration of DAKZS. As the tuning parameter approaches the critical point vs time, besides the conventional correlation time  $\zeta$  there is a time scale  $\zeta'$  characterizing the deconfinement process. The relevant time scale in DAKZS depends on the order parameter studied and the driving direction, as discussed in the text. The topological defects in the two ordered phases are illustrated; vortices with  $S = 1/2$  cores (spinons) and hedgehogs (monopoles) in the VBS and AFM phases, respectively. In the middle, deconfinement of two spinons (strings in a sampled QMC configuration of an  $S = 1$  state [24]) initially located at nearest-neighbor sites is illustrated for short and long annealing times. The dynamic scaling of the mean string length  $\Lambda$  (b) violates the conventional KZS with  $\zeta_v$ , while (c) satisfying DAKZS with  $\zeta'_v$  being the relevant time scale. The line has slope  $-1/r'$ , as expected for this scaling function when both  $vL^{r'}$  and  $L$  are large. Statistical errors here and in other figures are smaller than the symbol size.

annealing; driving the system from an initially ordered or disordered state. In a sufficiently large system ( $L \gg \xi_v$ ) annealed to  $g = 0$ , the scaling function must develop power-law behavior in  $vL^r$  such that  $L$  is either eliminated (when starting in the ordered phase) or  $P^2 \propto L^{-d}$  (approaching from the disordered phase in  $d$  dimensions),

$$P^2(v, L) \sim \begin{cases} v^{2\beta/\nu r}, & g_0 > 0, \\ L^{-d} v^{(2\beta-d\nu)/\nu r}, & g_0 < 0, \end{cases} \quad (3)$$

if  $g_0 > 0$  corresponds to an initially ordered state.

Applications of KZS range from cosmology to condensed matter and qubit arrays [25, 26, 33–38]. While classical KZS has been studied extensively using simulated (Monte Carlo) annealing [31, 32, 39, 40], testing predictions of quantum KZS [41–43] in models beyond 1D is in general challenging because solutions of the time dependent Schrödinger equation are limited to small system sizes [44]. However, for models accessible to quantum Monte Carlo simulations, KZS with identical exponents can be studied by annealing in imaginary time [30], as outlined in Appendix A and illustrated for quantum Ising models in Appendix B.

Here we will demonstrate that conventional KZS does not apply to DQC. Using a 2D quantum magnet with AFM and VBS ground states as an example, illustrated in Fig. 1, imaginary-time annealing shows that the deconfinement time scale  $\zeta' \propto \xi'^z$  affects the dynamic scaling of the order parameters in a way depending on the direction of the driving, i.e., from which ordered state the annealing process is started. The directionality further obeys a duality stemming from the topological defects in

the two phases. We construct an extension of KZS that we will refer to as dual asymmetric KZS (DAKZS).

Below we first define the spin model, then outline our DAKZS ansatz and demonstrate its validity using imaginary-time annealing; see Appendix A for technical details. As a contrast, we will also discuss classical simulated annealing of a three-dimensional (3D) clock model, which hosts a symmetry cross-over length  $\xi' \gg \xi$  but no second ordered phase generated by proliferation of topological defects. Therefore, conventional KZS describes the order parameter in this case.

**$JQ$  model.**—We study annealing dynamics of the spin-1/2  $JQ_3$  model [4, 6], with the Hamiltonian

$$H = -J \sum_{\langle ij \rangle} P_{ij} - Q \sum_{\langle ijklmn \rangle} P_{ij} P_{kl} P_{mn}, \quad (4)$$

where  $P_{ij} \equiv 1/4 - \mathbf{S}_i \cdot \mathbf{S}_j$  are singlet projectors and  $\langle ij \rangle$  and  $\langle ijklmn \rangle$  denote, respectively, nearest-neighbor sites and three nearest-neighbor pairs in both horizontal and vertical columns on the 2D square lattice. We take  $Q = 1$  as the unit of energy and change  $J$  versus imaginary time  $t$  under different driving protocols, starting from the ground state at some initial value  $J_0$  stochastically projected out of a trial state. The choice of initial state is discussed further in Appendix C.

Like the  $JQ_2$  model [4] (with two singlet projectors instead of three in the  $Q$  term), it was shown that the  $JQ_3$  model hosts AFM and columnar VBS order for large and small  $J$ , respectively, with the transition point

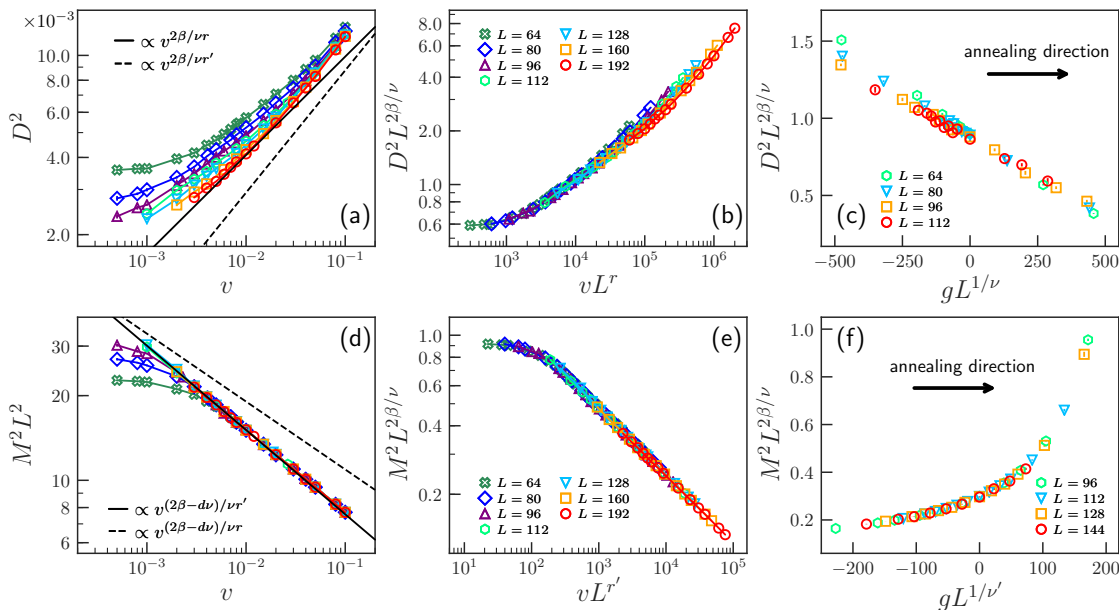


FIG. 2. **Annealing from the VBS side.** (a) Dependence of the VBS order parameter on the driving velocity  $v$  at the critical point for different system sizes [legends in (b)]. The solid line shows the power law  $D^2 \propto v^{2\beta/\nu r}$  fitted to the  $L = 192$  data, while the slope of the dashed line corresponds to the exponent when  $r \rightarrow r'$ . (b) Data collapse with  $v$  rescaled by  $L^r$  and  $D^2$  by  $L^{2\beta/\nu}$ . (c) For fixed  $vL^r = 5000$ , the scaled  $D^2$  data collapse for large  $L$  when  $g$  is rescaled by  $L^{1/\nu}$ . (d) The size-scaled AFM order parameter vs  $v$ . The solid line shows  $M^2 L^2 \propto v^{(2\beta-d\nu)/\nu r'}$  and the dashed line has slope corresponding to  $r' \rightarrow r$ . (e) Data collapse with  $v$  rescaled by  $L^{r'}$  and  $M^2$  by  $L^{2\beta/\nu}$ . (f) Data collapse at fixed  $vL^{r'} = 5000$  with  $g$  rescaled by  $L^{1/\nu'}$ .

$J_c \approx 0.671$  [6, 45] and a more robust VBS order for  $J = 0$  than the  $JQ_2$  model. While it is possible that the transition is ultimately weakly first-order [9, 46], the order-parameter discontinuities are too small to detect on lattice sizes up to  $L \approx 200$ . Consistency among different microscopic models [9, 47] suggests that the extracted critical exponents accurately reflect a nearby DQC point.

We compute the AFM order parameter

$$\mathbf{M} \equiv \frac{1}{L^2} \sum_r (-1)^{r_x+r_y} \mathbf{S}_r \quad (5)$$

and the VBS order parameter ( $D_x, D_y$ ) with

$$D_a \equiv \frac{1}{L^2} \sum_r (-1)^{r_a} (\mathbf{S}_r \cdot \mathbf{S}_{r+\hat{a}}), \quad \hat{a} = \hat{x}, \hat{y}. \quad (6)$$

We analyze the expectation values of the squares,  $M^2$  and  $D^2 = D_x^2 + D_y^2$ . The exponents of interest are  $\nu \approx 0.455$  [9, 47],  $z = 1$ , and the common [assuming emergent  $SO(5)$  symmetry] order parameter exponent  $\beta \approx 0.28$  [9, 45].

**Dynamic deconfinement.**—In addition to the conventional critical exponents, in  $JQ$  models the exponent governing the confinement length  $\xi' \propto |g|^{-\nu'}$  takes the value  $\nu' \approx 0.634 > \nu$  [11]. In an annealing process, one may then also expect a second time scale  $\zeta' = \xi'^z > \zeta$  (illustrated in Fig. 1) and a related length scale limited by finite annealing velocity. Thus, we will develop the phenomenological DAKZS ansatz based on the velocity

limited confinement length in analogy with Eq. (1);

$$\xi'_v \sim v^{-1/r'}, \quad r' \equiv z + 1/\nu'. \quad (7)$$

Before presenting the general DAKZS ansatz, we first confirm the dynamic scale  $\xi'_v$ . To this end, we investigate the deconfinement process of an initially local (at two neighboring sites) triplet excitation embedded in the VBS background, starting the annealing process of the  $JQ_3$  model deep inside its VBS phase, at  $J = 0$ , and ending at  $J = J_c$ . We monitor the size  $\Lambda$  of the spinon pair defined via the strings connecting unpaired spins in a singlet background in the valence-bond basis in the  $S = 1$  sector [11, 24]. As shown in Fig. 1(b),  $\Lambda/L$  data for different annealing velocities and system sizes graphed versus  $vL^r$  do not collapse well onto a common scaling function  $f_\Lambda(vL^r)$ . In contrast, as shown in Fig. 1(c), good data collapse is achieved by assuming  $\Lambda = L f_\Lambda(vL^{r'})$ . Then, for large  $vL^{r'}$  (and sufficiently large  $L$ ),  $f_\Lambda \propto (vL^{r'})^{-1/r'}$ ,  $\Lambda \propto \xi'_v \propto v^{-1/r'}$ , and we can also write

$$\Lambda(v, L) = v^{-1/r'} \tilde{f}_\Lambda(vL^{r'}). \quad (8)$$

This scaling form implies that the deconfinement process is adiabatic only when  $|t|$  exceeds the longer of the two divergent time scales illustrated in Fig. 1.

The appearance of two dynamic length scales qualitatively reshapes the KZS mechanism, leading us to formulate the DAKZS as follows: For a general observable  $Y$ ,

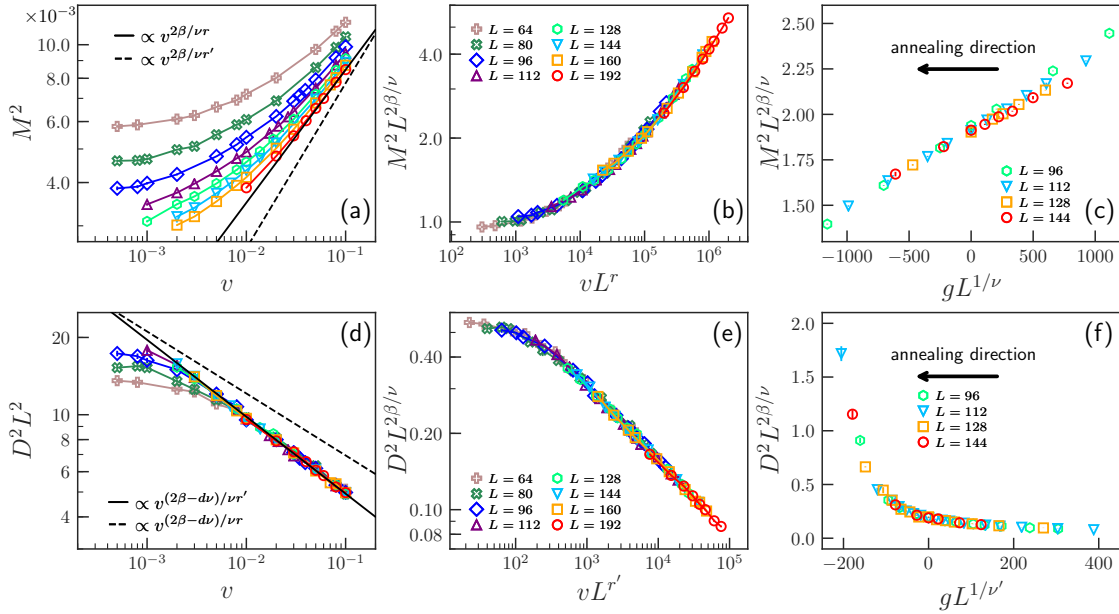


FIG. 3. **Annealing from the AFM side.** (a) The AFM order parameter  $M^2$  vs  $v$  at the critical point for different system sizes [legends in (b)]. The solid line shows the form  $M^2 \propto v^{2\beta/\nu r}$  with amplitude matching the  $L = 192$  data, while the dashed line shows the slope when  $r \rightarrow r'$ . (b) Data collapse when  $v$  is rescaled by  $L^r$  and  $M^2$  by  $L^{2\beta/\nu}$ . (c) Data at fixed  $vL^r = 75000$  collapse when for large  $L$   $g$  is rescaled by  $L^{1/\nu}$ . (d) The size-scaled VBS order parameter, with the form  $D^2 L^2 \propto v^{(2\beta-d\nu)/\nu r'}$  shown as the solid line; the dashed line corresponds to the exponent when  $r' \rightarrow r$ . (e) Data collapse when  $v$  is rescaled by  $L^{r'}$  and  $D^2$  by  $L^{2\beta/\nu}$ . (f) Scaled  $D^2$  data vs  $gL^{1/\nu'}$  for fixed  $vL^{r'} = 5000$ .

finite-size scaling in the vicinity of the transition at  $g = 0$  can be expressed as

$$Y(v, g, L) = L^{-\Delta} f_Y(vL^{\tilde{r}}, gL^{1/\tilde{\nu}}), \quad (9)$$

where  $\Delta$  is the scaling dimension of  $Y$  and  $\tilde{r}$  is either  $r$  or  $r'$ , depending on  $Y$  and the annealing direction (in a way that will be determined below); similarly,  $\tilde{\nu}$  should be  $\nu$  or  $\nu'$ . With  $\tilde{r} = r$  and  $\tilde{\nu} = \nu$ , the DAKZS ansatz reduces to the conventional KZS form Eq. (2).

We will reach the limit where  $L$  exceeds both  $\xi_v$  and  $\xi'_v$ , so that the system is essentially in the thermodynamic limit at  $g = 0$  and power laws developing for large scaling argument  $vL^{\tilde{r}}$  in Eq. (9) lead to forms analogous to Eq. (3). We will be far from the limit  $vL^{\tilde{r}} \rightarrow 0$  for large  $L$  and circumvent the issue of potential anomalous powers of  $L$  in equilibrium [9, 11]. The aim of the following analysis is to demonstrate how  $\tilde{r}$  and  $\tilde{\nu}$  in the case of the order parameters change with the annealing direction, reflecting the time scale of equilibration of topological defects and a duality between the AFM and VBS phases.

**Scaling of the order parameters.**—The equilibrium DQC theory posits a single exponent  $\nu$  governing the divergence of both the AFM and VBS correlation lengths in both phases [1, 2]. Therefore, one might expect conventional KZS controlled by  $\nu$  and  $z = 1$  to apply for both  $D^2(v, L)$  and  $M^2(v, L)$ , irrespective of the phase from which the critical point is approached.

Figure 2 shows results for the squared order param-

eters at  $J = J_c$  after annealing from the VBS phase at  $J = 0$ . The VBS order parameter in Fig. 2(a) indeed exhibits scaling behavior consistent with  $D^2 \propto v^{2\beta/\nu r}$ , as in the first line of Eq. (3), for small  $v$  and sufficiently large  $L$ . Figures 2(b) and 2(c) show that the variables in the scaling function are  $vL^r$  and  $gL^{1/\nu}$ ; thus  $D^2$  satisfies the conventional KZS form Eq. (2).

In contrast, Fig. 2(d) shows that the short-ranged AFM order parameter in the VBS phase is governed by the confinement scale, having the form  $M^2 L^2 \propto v^{(2\beta-d\nu)/\nu r'}$  (shown with the solid line), as on the second line of Eq. (3) but with  $r \rightarrow r'$ . The velocity scaling is very consistent for all the system sizes before the cross-over toward the  $v$ -independent equilibrium value. Conventional KZS governed by the exponent  $r$  (slope indicated by the dashed line) can be excluded. As shown in Figs. 2(e) and 2(f),  $r'$  is also established as the correct exponent in more comprehensive data analysis at both  $g = 0$  and  $g \neq 0$ .

To explain why the growth of AFM correlations is slower, governed by  $\zeta'$ , we can invoke the topological defects: the spinons that deconfine on the same time scale according to Fig. 1(c). The AFM correlations in the VBS are directly related to the  $S = 1/2$  carrying spinons (which condense in the AFM phase) in the singlet background, and our results imply that it is only when the spinons have equilibrated that the critical AFM correlations can form. Thus, unlike the ground state, where the AFM correlation length is  $\xi$ , the annealing process ex-

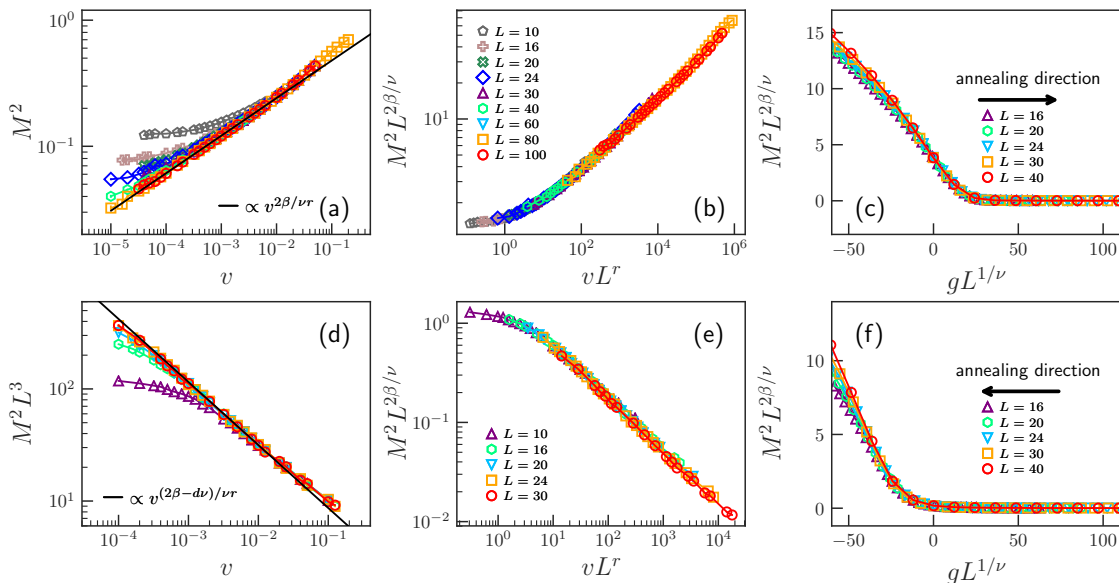


FIG. 4. **Conventional KZS in the classical  $q = 6$  clock model.** Upper row: Results for the average squared magnetization after linear simulated annealing to  $T_c \approx 2.20201$  [48] from the ordered phase at  $T_0 = T_c - 2$  (the coupling  $J = 1$ ). (a) Dependence of  $M^2$  on  $v$  for different system sizes [legends in (b)]. The line indicates the expected power law  $\propto v^{2\beta/\nu r}$  with 3D XY exponents. (b) Collapse of the data of (a) after rescaling as  $M^2 L^{2\beta/\nu}$  vs  $vL^r$ . (c) Data collapse in the vicinity of  $g = 0$  at fixed  $vL^r = 100$  and  $g$  rescaled by  $L^{1/\nu}$ . Lower row: Results at  $T_c$  after annealing from the paramagnetic phase at  $T_0 = T_c + 2$ . (d) Volume-scaled  $M^2$  vs  $v$  for different system sizes [legends in (e)]. The line indicates the expected power law  $\propto v^{(2\beta-d\nu)/\nu r}$  for small  $v$  and large  $L$ . (e) Data collapse after rescaling to  $M^2 L^{2\beta/\nu}$  vs  $vL^r$ . (f) Data collapse with  $g$  rescaled to  $gL^{1/\nu}$  at fixed  $vL^r = 100$ . For details of these simulations and additional results, see Appendix D.

poses the spinon dynamics and the larger scale explicitly in  $M^2$ . The VBS order parameter has already equilibrated at the shorter time scale  $\zeta$  and is insensitive to the deconfinement scale as far as its amplitude is concerned [while the second scale should enter in the  $Z_4$  to  $U(1)$  cross-over [2], which we do not discuss here]. This dynamic asymmetry between the order parameters is one of the defining aspects of DAKZS.

A second remarkable aspect of DAKZS is the duality manifested when the annealing direction is reversed. To observe the duality, we turn to an annealing process starting in the AFM state at  $J = 1.2$  and reducing the value at different velocities to  $J_c$ . Figure 3 shows results for the two order parameters analyzed in analogy with Fig. 2. Here the AFM order parameter obeys the conventional KZS form with the exponent  $r$ , while the short-ranged VBS order parameter is controlled by  $r'$ .

Owing to the emergent  $SO(5)$  symmetry of the DQC point [10, 23], a duality between the AFM and VBS order parameters in equilibrium is expected. Our results demonstrate a dynamic duality between the topological defects, with the longer deconfinement scale not only controlling the equilibration of spinons in the VBS phase but also the hedgehog defects in the AFM phase, which must reach equilibrium before the critical VBS correlations can form in the AFM background, thus requiring the time scale  $\zeta'$ . The AFM order equilibrates on the faster scale  $\zeta$ .

**Clock model.**—The profound implications of DAKZS are further highlighted by comparing DQC dynamics and the stochastic (Monte Carlo) dynamics of 3D classical  $q$ -state clock models. For  $q \geq 4$  they exhibit  $U(1) \rightarrow Z_q$  cross-over of the order parameter symmetry at a length scale  $\xi'_q$  controlled by an exponent  $\nu_q > \nu$  [48, 49]. However, the topological defects in this case do not have any internal structure analogous to the  $S = 1/2$  cores of the VBS vortices, and there is no second order parameter generated by proliferation of defects—instead the clock model transitions into a trivial paramagnetic phase above the critical temperature  $T_c$ .

We have studied the  $q = 6$  clock model using classical simulated annealing. As shown in Fig. 4, the squared order parameter is indeed fully described by conventional KZS with 3D XY exponents, with no sign of any second scale controlled by  $\nu'_6 \approx 1.52 > \nu \approx 0.67$  [48]. As discussed in detail in Appendix D., the second scale does appear in a quantity directly probing the  $Z_q$  symmetry, which can be analyzed with a KZS-inspired generalization of the equilibrium two-length scaling formalism developed in Ref. [48].

**Conclusions.**—Our numerical simulations have uncovered additional richness of the DQC phenomenon that was not anticipated in previous works. The dynamic scaling ansatz that we call DAKZS can be summarized by replacing  $r = z + 1/\nu$  on the second line of Eq. (3) by  $r' = z + 1/\nu'$  when  $P$  is the order parameter that



is not long-ranged in the phase from which the annealing is started, becoming long-ranged on the other side of the transition. Calling said (dis)order parameter  $P_{\text{dis}}$ , its scaling form including also the behavior slightly inside the phases can be written as a specific case of the general form Eq. (9) combined with analogue of the second of the asymptotic forms in Eq. (3);

$$P_{\text{dis}}^2(v, L) = L^{-d} v^{(2\beta - d\nu)/\nu r'} \tilde{f}_P(vL^{r'}, gL^{1/\nu'}). \quad (10)$$

Equilibrium critical scaling  $P_{\text{dis}}^2 \propto L^{-2\beta/\nu}$  can be recovered from this form when  $g = 0$  and  $v \rightarrow 0$  (by the scaling function  $\tilde{f}_P$  developing a power-law form). However, recovery of the correct equilibrium scaling  $|g|^{2\beta}$  when  $P_{\text{dis}}$  becomes long-ranged requires another argument  $gL^{1/\nu}$  of  $f_P$  to become important in the asymptotic low- $v$  limit, which we have not considered here (but similar asymptotics are discussed in the context of the clock model in Appendix D.). The good scaling collapses in Figs. 2(f) and 3(f) indicate that Eq. (10) works well on both sides of the transition before the equilibrium behavior sets in.

The comparison with the classical clock model in Fig. 4 demonstrates explicitly that a second time scale is not always manifested in the order parameter. The complex topological defects expose the second dynamic scale in the case of DQC, which can be most easily understood from the perspective of the  $S = 1/2$  cores of the VBS vortices [2]. It is the build-up of correlations among these  $S = 1/2$  objects that require the longer time scale, and, invoking our annealing results and the proposed duality between the two ground-state phases [3, 13], we posit that equilibration of hedgehogs in the AFM phase is also governed by the same longer time scale.

Dualities and topological defects are at the heart of many exotic quantum phases and transitions of interest in studies of exotic quantum matter [13, 19, 20, 22]. Our DAKZS ansatz opens a window beyond KZS to emergent topological degrees of freedom through their dynamics out of equilibrium. Noting that arrays of controllable Rydberg atoms provide a platform to realize both exotic quantum phases and driven dynamics [37], our scaling approach can potentially be directly exploited in that context in the near future.

**Acknowledgements.**—We would like to thank T. Senthil for valuable discussions. S.Y. is supported by the National Natural Science Foundation of China, Grants No. 12222515 and No. 12075324. Y.-R.S. is supported by the National Natural Science Foundation of China, Grant No. 12104109 and Key Discipline of Materials Science and Engineering, Bureau of Education of Guangzhou, Grant No. 202255464. S.-K.J. is supported by a startup fund at Tulane University. A.W.S. is supported by the Simons Foundation under Grant No. 511064. The numerical simulations here were carried out on the TianHe-2 (the National Supercomputer Center in Guangzhou) and a cluster built in collaboration with Guangzhou Ginpie Technology Co., Ltd. Some test cases were run on the

Shared Computing Cluster managed by Boston University's Research Computing Services.

## Appendix A: Methods

The numerical quantum annealing results were obtained using the nonequilibrium quantum Monte Carlo (NEQMC) method [30], which is a further development of the projector quantum Monte Carlo (QMC) method. Implementing Schrödinger dynamics for a time dependent Hamiltonian in imaginary time, it reproduces the same critical behavior (exponents) as in real time when annealing toward a critical point [30, 50]. We here briefly outline the NEQMC method [30, 51] and provide results for benchmark cases in Appendix B.

For a given imaginary-time (for which we now use the symbol  $\tau$  instead of  $t$  in the main text) dependent Hamiltonian  $H(\tau)$ , the evolution of a state obeys the analogue of Schrödinger dynamics,  $|\psi(\tau)\rangle = U(\tau)|\psi(\tau_0)\rangle$  (up to an unimportant normalization constant), where  $|\psi(\tau_0)\rangle$  is the initial state and

$$U(\tau) = T_\tau \exp \left[ - \int_{\tau_0}^{\tau} d\tau' H(\tau') \right], \quad (A1)$$

is the Euclidean time evolution operator, with  $T_\tau$  imposing time ordering.

In the NEQMC method,  $U(\tau)$  is expanded in a power-series and applied to the initial state  $|\psi(\tau_0)\rangle$ , giving

$$|\psi(\tau_a)\rangle = \sum_{n=0}^{\infty} \int_{\tau_0}^{\tau_a} d\tau_n \int_{\tau_0}^{\tau_n} d\tau_{n-1} \cdots \int_{\tau_0}^{\tau_3} d\tau_2 \int_{\tau_0}^{\tau_2} d\tau_1 \times [-H(\tau_n)] \cdots [-H(\tau_1)] |\psi(\tau_0)\rangle, \quad (A2)$$

where we now denote the final annealing time  $\tau_a$  (which with  $\tau_0 = 0$  is the total annealing time). After inserting additional time integrals over unit operators  $H_0$  at  $m - n$  locations, with  $m$  representing a truncation of the infinite series, and splitting the Hamiltonian into bond (or other lattice units, e.g., the six-spin cells of the  $Q_3$  interaction) operators,

$$H = - \sum_{b=1}^{N_b} H_b, \quad (A3)$$

the state (whose normalization is irrelevant for Monte Carlo sampling) can be written as

$$|\psi(\tau_a)\rangle = \sum_{S_m} \frac{(m-n)!}{(\tau_a - \tau_0)^{m-n}} \int_{\tau_0}^{\tau_a} d\tau_n \int_{\tau_0}^{\tau_n} d\tau_{n-1} \cdots \cdots \int_{\tau_0}^{\tau_3} d\tau_2 \int_{\tau_0}^{\tau_2} d\tau_1 S_m |\psi(\tau_0)\rangle, \quad (A4)$$

in which  $S_m$  denotes the operator sequence,

$$S_m = \prod_{i=1}^m H_{b_i}(\tau_i), \quad (A5)$$

and  $n$  is the number of non-unit operators;  $b_i \neq 0$ . The factor before the integrals in Eq. (A4) corrects for the integration volume and number of possible insertions of the  $m - n$  unit operators  $H_0$ . The truncation  $m$  of the expansion must scale as  $m \propto L^d(\tau_a - \tau_0)$  and is adapted self-consistently during the equilibration stage of the simulation, thus causing only a vanishingly small truncation error (as in the finite-temperature stochastic series expansion method [52]).

To implement importance sampling of the normalization  $Z = \langle \psi(\tau_a) | \psi(\tau_a) \rangle$ , the wave function is written in a basis  $\{|\alpha\rangle\}$ , which for  $S = 1/2$  models with spin-isotropic interactions, like the  $JQ$  models, can be conveniently taken to be the overcomplete valence-bond basis [4, 53, 54]. In this work we use the valence bond basis for the  $JQ_3$  model, while the transverse-field Ising models (see Appendix B.) are simulated in the conventional spin- $z$  basis as in Refs. [30, 51].

A full Monte Carlo sweep of the importance sampling procedure consists of updates of  $S_m$ ,  $\tau_m$  and the basis state  $\{|\alpha\rangle\}$ . The updates of  $S_m$  and  $\{|\alpha\rangle\}$  are carried out first, with the time value  $\tau_m$  fixed. The ordered time values can be sampled without changing  $S_m$  and  $\{|\alpha\rangle\}$  in separate updates alternating with those of the operator sequence and the states.

The updates of  $S_m$  and  $\{|\alpha\rangle\}$  are mostly the same as those in standard projector QMC and the stochastic series expansion QMC method [52, 53], except that the probabilities of different types of operators are now associated with time values  $\tau_m$  that enter in the probabilities for the diagonal operator updates in each propagation step in the imaginary-time direction.

To sample the time integrals in Eq. (A4) efficiently, a multi-point update scheme is used. A random segment  $\{\tau_i, \dots, \tau_{i+n_\tau}\}$  of time values is first chosen, with  $n_\tau$  the length of the segment. Then random numbers in the range  $(\tau_{i-1}, \tau_{i+n_\tau+1})$  are generated and ordered, leading to a new allowed and unbiased time set  $\{\tau'_i, \dots, \tau'_{i+n_\tau}\}$ . The Metropolis acceptance probability to replace the chosen time set with the new set can be easily obtained from Eq. (A4). The length of the segment  $n_\tau$  is adjusted to maintain a reasonable mean acceptance rate, close to 1/2.

Measurements of expectation values of operators  $A$  are taken in the middle of the double-sided projection;

$$\langle A(\tau_a) \rangle = \frac{1}{Z} \langle \psi(\tau_a) | A | \psi(\tau_a) \rangle. \quad (\text{A6})$$

For the estimators expressed in the generated configurations in the valence-bond basis, we refer to the literature, e.g., Ref. [54].

In some systems (like those in Appendix B) it is convenient to use simple initial states that are trivially eigenstates of appropriate starting Hamiltonians. With the  $JQ$  models, there are no such simple eigenstates close to the AFM–VBS transition. To generate initial states, we therefore carry out additional projections (as a part of the overall time evolution) with the Hamiltonian fixed at its initial parameters before the time dependence is applied, i.e., in the initial stages of Eq. (A4) up to some

sufficiently long time, the Hamiltonian is not dependent on  $\tau$  (and the integrals can therefore also be eliminated). The final sampled state of these additional projections then effectively serves as the initial state  $|\psi(\tau_0)\rangle$  to which the successive driving (with the time dependent Hamiltonian) is applied.

In the case of the  $JQ_3$  model, we always fix  $Q = 1$ , take the initial time in Eq. (A4) as  $\tau_0 = 0$  [when the time dependent interactions is turned on after initial projection with fixed  $H(J_0)$ ], and evolve with  $\tau > 0$ . For the VBS initial state,  $J_0 = 0$ , the driving parameter  $J$  is increased following  $J(\tau) = J_0 + v\tau$ , while with the AFM initial state,  $J_0 = 1.2$ ,  $J$  varies according to  $J(\tau) = J_0 - v\tau$ . In calculations with  $g = 0$ , the final time value is  $\tau_a = |J_c - J_0|/v$ , and when stopping at  $g \neq 0$  the corresponding final  $J$  value replaces  $J_c$ . Note that  $J(\tau) \geq 0$  must be satisfied in order to maintain the interactions antiferromagnetic—for negative  $J$  the simulations are affected by a sign problem.

## Appendix B: Conventional KZS in quantum Ising models

The quantum Ising model (the transverse-field Ising model) serves as a testing ground for a variety of theories, experiments, and numerical simulations in the study of quantum critical phenomena. The Hamiltonian defined on an arbitrary lattice with nearest-neighbor site pairs  $\langle ij \rangle$  is

$$H = -J \sum_{\langle ij \rangle} \sigma_i^z \sigma_j^z - h \sum_i \sigma_i^x, \quad (\text{A1})$$

where  $\sigma_i^x, \sigma_i^z$  are Pauli matrices,  $J > 0$  is a ferromagnetic coupling, and  $h$  is the strength of the transverse field.

The 1D version of the model can be solved exactly [55]. It hosts a quantum phase transition between the ferromagnetic and paramagnetic phases at the coupling ratio  $(h/J)_c = 1$ . The critical exponents for the order parameter and the correlation length are  $\beta = 1/8$  and  $\nu = 1$ , respectively, following from the mapping to a 2D classical model [56–58]. The 2D model has no rigorous analytical solution. Recent numerical simulations have placed the critical point at  $(h/J)_c \approx 3.04451$  on a square lattice, and the universality class is again that of the classical model in one higher dimension, with the critical exponents  $\beta \approx 0.3258$  and  $\nu \approx 0.6289$  [51, 59, 60]. The dynamic exponent is  $z = 1$  for both the 1D and 2D models, reflecting the emergent Lorentz invariance of the model when mapped to the  $D + 1$  dimensional classical model.

The driven dynamics of the quantum Ising model obeys conventional KZS, and it has been confirmed in previous studies that imaginary-time dynamics results in the same type of scaling behavior as in real time [30, 50]. Starting an annealing process from the ordered side of the transition, the leading scaling form of the order parameter is

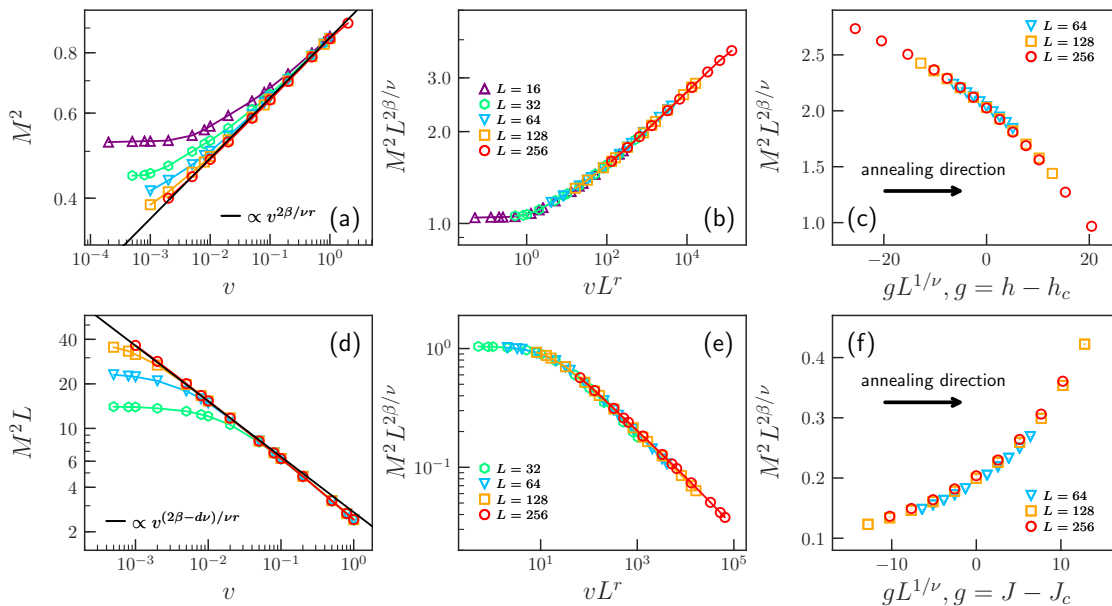


FIG. A1. **KZS in the 1D quantum Ising model.** Upper row: Annealing from the ordered phase to the critical point. (a) Dependence of  $M^2$  on  $v$  for  $L = 16$  to  $256$  [legends in (b)]. The solid line indicates the power law  $v^{2\beta/\nu r}$  applicable for large  $L$  and small  $v$ . (b) Rescaling  $v$  and  $M^2$  as  $vL^r$  and  $M^2 L^{2\beta/\nu}$ , respectively, leads to data collapse as expected. (c) Data collapse after rescaling  $M^2$  versus  $g$  in the driving process for  $L = 64$  to  $256$  at fixed  $vL^r = 1000$ . Lower row: driving from the disordered phase. (d) Dependence of the size-scaled  $M^2$  on  $v$  at the critical point for  $L = 32$  to  $256$ . The solid line shows the power law  $v^{(2\beta-d\nu)/\nu r}$  expected for large  $L$  and small  $v$ . (e) Rescaling  $v$  and  $M^2$  as  $vL^r$  and  $M^2 L^{2\beta/\nu}$ , respectively, for data collapse. (f) Rescaled  $M^2$  versus  $g$  for  $L = 64$  to  $256$  at fixed  $vL^r = 1000$ . All results support the KZS mechanism.

[31, 32, 39, 61]

$$M^2(v, L) = v^{2\beta/\nu r} f_M(vL^r, gL^{1/\nu}), \quad (\text{A2})$$

in which  $r = z + 1/\nu$ ,  $g$  is the distance to the critical point, and  $v$  the driving velocity. In contrast, starting from the paramagnetic side, the scaling form is

$$M^2(v, L) = L^{-d} v^{(2\beta-d\nu)/\nu r} f_M(vL^r, gL^{1/\nu}), \quad (\text{A3})$$

though the form of the scaling function  $f_M$  is not the same as in Eq. (A2). Note, however, that although Eqs. (A2) and (A3) have different leading terms when expressed in the annealing velocity, both of them can be converted into the form

$$M^2(v, L) = L^{-2\beta/\nu} f_M(vL^r, gL^{1/\nu}), \quad (\text{A4})$$

by redefining  $f_M$  by extracting appropriate power laws of the argument  $vL^r$  from the scaling function [as was argued in reverse in the main text, Eqs. (2) and (3)]. Either of the forms can be used for analyzing data for different velocities and system sizes.

We perform NEQMC simulations [30] (also see Appendix A) of both the 1D and 2D quantum Ising models. For the ordered initial state, the driving protocol is  $h = h_0 + v\tau$  with  $J = 1$  and  $h_0 = 0$ , such that the initial state can be prepared by setting all spins aligned ferromagnetically in the  $z$  direction. Here, the distance to the critical point is defined as  $g \equiv h - h_c$ . Therefore,

driving the system to the critical point corresponds to linearly varying  $h$  versus  $\tau$  from 0 to the critical value  $h_c = 1$  [56–58] and  $3.04451$  [51, 59] for the 1D and 2D case, respectively.

For the disordered initial state, instead of driving  $h$ , we choose  $J = J_0 + v\tau$  with  $h = 1$  and  $J_0 = 0$ , such that the initial state can be easily prepared with the equal superposition of all spin- $z$  basis state;

$$|\psi(\tau_0)\rangle = \bigotimes_{i=1}^{L^d} (|\uparrow\rangle_i + |\downarrow\rangle_i). \quad (\text{A5})$$

This initial state is sampled collectively along with the evolved states as dictated by the operators in the product  $S_m$  in Eq. (14) in Appendix A.

Driving the system to the critical point then means  $J$  evolving from  $J_0 = 0$  to  $J_c = 1$  and  $0.32846$  for the 1D and 2D case, respectively. Here the distance to the critical point is defined as  $g \equiv J - J_c$ . The previous NEQMC simulations only considered the paramagnetic initial state [30, 50]. A “two-way” projection with mixed time boundaries was also considered with a slightly different algorithm [51]. The results presented here for both annealing directions extend to lower velocities and larger system sizes.

For the 1D case, we show results starting from the ferromagnetic initial state in the upper row of Fig. A1. At the critical point  $g = 0$ , Fig. A1(a) shows that  $M^2$  decreases as  $v$  decreases. For a finite-size systems, as



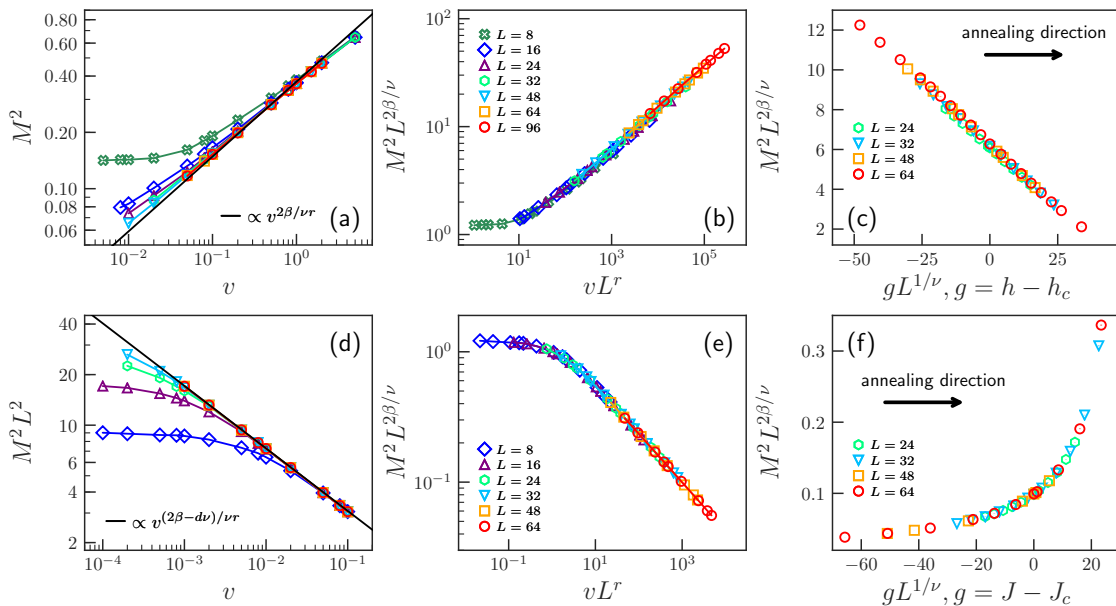


FIG. A2. **KZS in the 2D quantum Ising model.** Upper row: driving from the ordered phase. (a) Dependence of  $M^2$  on  $v$  at the critical point for  $L = 8$  to  $96$ . The solid line indicates the form  $v^{2\beta/\nu r}$ . (b) Data collapse with  $v$  and  $M^2$  scaled by  $vL^r$  and  $M^2 L^{2\beta/\nu}$ , respectively. The solid line shows the power law  $(vL^r)^x$  with the expected exponent  $x = 2\beta/\nu r$ . (c) Data collapse with the expected powers of  $L$  in the neighborhood of the critical field at fixed  $vL^r = 1000$ . Lower row: driving from the disordered phase. (d) Dependence of the size-scaled  $M^2$  on  $v$  at the critical point for  $L = 8$  to  $64$ . The solid line shows the expected power law  $v^{(2\beta-d\nu)/\nu r}$  when  $L$  is sufficiently large. (e) Data collapse of  $vL^r$  versus  $M^2 L^{2\beta/\nu}$ . (f) Data collapse with the expected powers of  $L$  in the neighborhood of the critical coupling at fixed  $vL^r = 1000$ . All results support the KZS mechanism with the expected critical exponents.

$v \rightarrow 0$ ,  $M^2$  converges to its equilibrium size-dependent critical value,  $M^2 \propto L^{-2\beta/\nu}$ , as is explicit in Eq. (A4) with an analytic scaling function  $f_M$ . For larger  $v$ ,  $M^2$  obeys  $M^2 \propto v^{2\beta/\nu r}$ , as explicitly conveyed by Eq. (A2), where the scaling function  $f_M$  must approach a constant for large argument  $vL^r$ , as seen in Fig. A1(a). The form with only  $v$  dependence and no size corrections from the scaling function requires  $L$  to be sufficiently large,  $L \gg \xi_v$ . Furthermore, the correlation length should also obey  $\xi_v \gg 1$ , so that the system has evolved from the initial state and critical fluctuations have developed. After rescaling  $v$  and  $M^2$  as  $vL^r$  and  $M^2 L^{2\beta/\nu}$ , respectively, we observe in Fig. A1(b) that all data collapse well, as predicted by Eq. (A4) when  $g = 0$ .

In Fig. A1(c), we show that the rescaled curves of  $M^2$  versus  $g$  in the vicinity of the critical point also collapse onto each other for a fixed value  $vL^r$ , in which case Eq. (A4) again reduces to a single-variable scaling form. These results demonstrate that, in the 1D quantum Ising model,  $M^2$  evolving from the ordered initial state satisfies Eqs. (A2) and (A4), as expected [31, 32, 39, 61].

In the lower row of Fig. A1, we show results obtained when driving from the disordered paramagnetic phase. In Fig. A1(d), at the critical point  $M^2$  satisfies  $M^2 \propto v^{(2\beta-d\nu)/\nu r}$  for small  $v$  and large  $L$ , as predicted by Eq. (A3). After rescaling with the critical power of  $L$ , Fig. A1(e) shows that the data versus  $vL^r$  for different system sizes collapse onto a common scaling function to

a high degree, again as expected from the KZS mechanism expressed in the form of Eq. (A4). In Fig. A1(f), rescaled curves of  $M^2$  versus  $g$  for fixed  $vL^r$  are shown to collapse almost perfectly for  $L = 128$  and  $L = 256$ , while for  $L = 64$  small scaling corrections are visible. These results confirm the scaling forms in Eqs. (A3) and (A4) [32, 39, 61].

For the 2D case, similar results are shown in Fig. A2 and there is no need to comment further on these other than to conclude that KZS works extremely well also in this case, with almost no scaling corrections visible.

### Appendix C: Upper bound for the annealing velocity in the $JQ_3$ model

KZS requires that the system evolves adiabatically before the critical region, ideally starting from an eigenstate of the initial Hamiltonian (though this is strictly speaking not necessary in imaginary time, as long as the driving velocity is not too large given the initial parameters). Since a fast annealed system is dominated by the initial conditions, there is some upper bound on  $v$  above which scaling cannot be observed.

In this section, we determine the upper bound of the driving velocity, below which the effects induced by the initial state can be ignored when the initial driven parameter is far from the critical point. For the VBS ini-

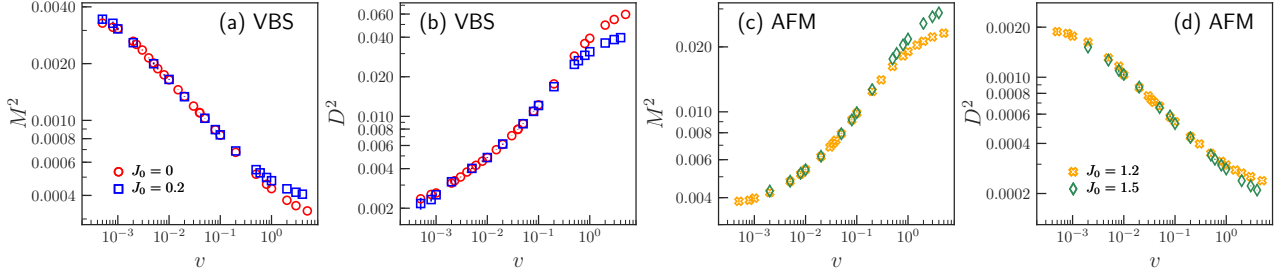


FIG. A3. **Determination of upper bound of  $v$ .** Curves of  $M^2$  in (a) and  $D^2$  in (b) vs  $v$  at the critical point starting from a VBS ground states with  $J_0 = 0$  and  $0.2$  for system size of  $L = 96$ . For the two initial states,  $M^2$  is statistically indistinguishable when  $v < 10^{-1}$ , and the same applies to  $D^2$  as well. Curves of  $M^2$  in (c) and  $D^2$  in (d) vs  $v$  at the critical point starting from an AFM ground states with  $J_0 = 1.2$  and  $1.5$  for  $L = 96$ . For  $v < 10^{-1}$ , both  $M^2$  and  $D^2$  agree for the two different initial states. The results of  $J_0 = 0$  and  $1.2$  are from the main text.

tial state, in the main text we use  $J_0 = 0, Q = 1$  and let  $J = J_0 + v\tau$ . Here we choose  $J_0 = 0.2$  and perform NEQMC simulations on a system with  $L = 96$ . As shown in Figs. A3(a) and A3(b), for both  $M^2$  and  $D^2$ , the differences between different initial states are small in the region of  $v < 10^{-1}$ . Similarly, for the AFM initial state, we compare the results starting from  $J_0 = 1.5, Q = 1$  with those starting from  $J_0 = 1.2, Q = 1$  (used in the main text) for  $L = 96$ . As shown in Figs. A3(c) and A3(d), curves of  $M^2$  and  $D^2$  versus  $v$  match each other for different initial states when  $v < 10^{-1}$ . Therefore, in the main text, the driving velocity  $v$  is chosen to be smaller than  $10^{-1}$  to guarantee that the effects induced by the initial state are negligible.

In principle, it would always be better to start further away from the critical point. However, for a fixed velocity  $v$ , a larger range of the annealing parameter implies slower simulations. While the projection of the initial state also takes time, it is faster than the annealing stage. Our choice of initial condition represents a compromise between simulation efficiency and range of  $v$  not affected by the initial state.

#### Appendix D: Extended KZS in 3D classical $Z_q$ -clock models

In this section, we explore driven stochastic (Metropolis Monte Carlo) dynamics in the classical  $Z_q$ -clock model on the 3D simple cubic lattice. The Hamiltonian of this model is

$$H = -J \sum_{\langle i,j \rangle} \cos(\theta_i - \theta_j) - h \sum_i \cos(q\theta_i), \quad (\text{A1})$$

in which  $\theta \in [0, 2\pi)$  and  $\langle i, j \rangle$  denotes nearest neighbors. Although the system only has the discrete  $Z_q$  symmetry, it was shown that, for  $q \geq 4$ , the phase transition for  $h \neq 0$  at temperature  $T = T_c$  belongs to the 3D  $U(1)$  universality class, which means  $h$  is irrelevant at the critical point [48, 62, 63]. The critical exponents for the order parameter and the correlation length are therefore

$\beta \approx 0.3485$  [64] and  $\nu \approx 0.6717$  [48]. However, in the ordered phase for  $T < T_c$ ,  $h$  is relevant, reducing the order parameter symmetry from  $U(1)$  to  $Z_q$ . Accordingly,  $h$  is categorized as a dangerously irrelevant scaling variable [48, 49, 62–77]. Thus, besides the usual correlation length  $\xi$ , there is another relevant length scale  $\xi^l$  that characterizes the cross-over from  $U(1)$  to  $Z_q$  symmetry of the order parameter (and also the thickness of domain walls). This second length scale  $\xi^l$  is governed by the exponent  $\nu' > \nu$  so that  $\xi^l \gg \xi$  upon approaching the critical point.

In the following, we take  $q = 6$  as an example to explore the critical dynamics of the model. In this case,  $\nu' \approx 1.52$  [48, 70]. We take the “hard clock” limit  $h \rightarrow \infty$  in Eq. (A1), implemented as a discrete set of  $q = 6$  sampled angles. The critical temperature in this case in units of the coupling,  $J = 1$ , is  $T_c \approx 2.20201$  [48]. We perform Monte Carlo simulations using standard Metropolis dynamics, in which case the dynamic exponent  $z \approx 2.00$  [78] (we use  $z = 2$  exactly). When starting the annealing process from the ordered state, the driving protocol is given by  $T = T_0 + vt$  with  $T_0 = 0.20201$ , while from the disordered state we take  $T = T_0 - vt$  with  $T_0 = 4.20201$  (i.e., the initial temperatures represent  $T_c/J \pm 2$ ). The annealing procedure in each case is repeated many (thousands or more) times and averages are taken over the final configurations at  $T_c$ .

In analogy with the  $JQ_3$  model in the main text, in the driven dynamics it is expected that there exists another characteristic velocity-limited length scale  $\xi'_v \propto v^{-1/r'}$  with  $r' = z + 1/\nu'$ , in addition to the usual typical length scale  $\xi_v \propto v^{-1/r}$  with  $r = z + 1/\nu$  in KZS. As the results in Fig. 4 of the main text show, the magnitude of the order parameter (the magnetization) is not affected by the longer scale and is described by conventional KZS. To reveal the second scale and develop an extended KZS formalism depending on it, we explore the annealing dynamics of an angular order parameter  $\phi_q$ , defined by

$$\phi_q \equiv \langle \cos(q\Theta) \rangle, \quad (\text{A2})$$

with  $\Theta = \arccos(M_x/M)$ , in which  $M = (M_x^2 + M_y^2)^{1/2}$

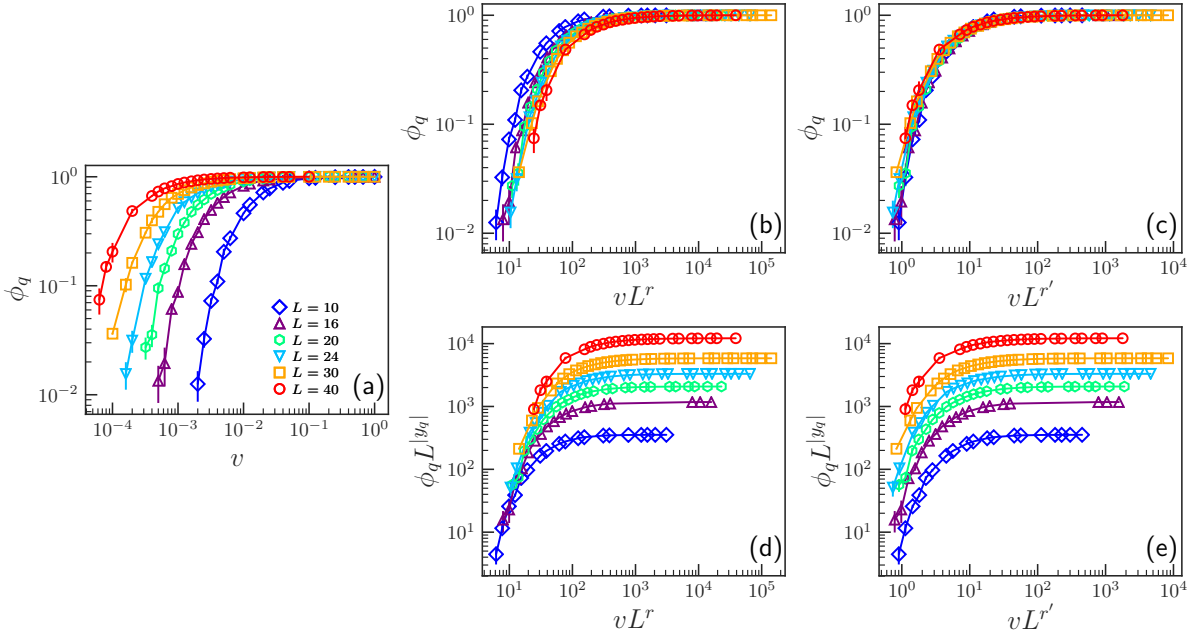


FIG. A4. **Dynamic scaling of the angular order parameter  $\phi_q$  ( $q = 6$ ); annealing from the ordered state.** (a) Dependence of  $\phi_q$  on  $v$  for system of size  $L = 10$  to  $40$ , starting from the ordered state at  $T_0 = T_c - 2 = 0.20201$ . (b) Rescaling  $v$  as  $vL^r$  does not collapse data for  $\phi_q < 1$ . (c) Rescaling  $v$  as  $vL^{r'}$  leads to good data collapse when  $\phi_q$  is close to 1. (d) Closer to equilibrium  $\phi_q$  should have scaling dimension  $y_q$  and rescaling with  $L^{|y_q|}$  indeed leads to data for small values of  $\phi_q L^{|y_q|}$  vs  $vL^r$ . (e) In contrast, there is no data collapse vs  $vL^r$ .

with

$$M_x = \frac{1}{L^3} \sum_i \cos(\theta_i), \quad M_y = \frac{1}{L^3} \sum_i \sin(\theta_i). \quad (\text{A3})$$

This angular order parameter and variations of it have been used in numerous equilibrium studies [48, 63, 65, 66, 70]. We here investigate the corresponding dynamical critical behavior.

Under external driving from the ordered initial state, Fig. A4(a) shows the dependence of  $\phi_q$  on the driving velocity  $v$  after reaching the critical point. Figure A4(b) shows that, after rescaling  $v$  as  $vL^r$  following KZS with the conventional correlation-length exponent  $\xi$ , the rescaled curves do not match each other, whereas rescaling as  $vL^{r'}$  in Fig. A4(c) leads to good data collapse. In this case we have not applied any rescaling to  $\phi_q$ , as it should be regarded as a dimensionless quantity in the regime where it is approaching the saturation value  $\phi_q = 1$  [48] (as discussed in more detail further below). In contrast, when  $\phi_q$  is small and size-dependent, i.e., when it is governed by its critical scaling dimension  $y_6 \approx -2.55$  [48, 66], it should be rescaled correspondingly to observe data collapse.

As shown in Fig. A4(d), with the critical rescaling we observe satisfactory data collapse for the smallest values of the velocity when graphing versus  $vL^r$  with the conventional KZS exponent  $r = z + 1/\nu$ . Because of difficulties in obtaining good data for large systems at low velocity, we cannot unambiguously claim that the

asymptotic small- $vL^r$  scaling in Fig. A4(d) is better than that in Fig. A4(c) for small  $vL^{r'}$ , but the data are at least consistent with  $r$  controlling the near-equilibrium critical behavior. If we instead rescale as  $vL^{r'}$ , there is no apparent data collapse at all, as seen in Fig. A4(e). Thus, we conclude that the conventional KZS mechanism most likely applies for small driving velocity, where  $\phi_q$  decreases versus the system size, while for larger driving velocity, where  $\phi_q$  is effectively dimensionless because of the ordered and symmetry-broken initial state, an extended KZS mechanism applies that is governed by the exponent  $r' = z + 1/\nu'$ .

The extended KZS mechanism at play in the clock model is still different from the DAKZS of the  $JQ_3$  model, where there are two ordered states and a duality between the two order parameters and their topological defects. We have not investigated any angular order parameter analogous to  $\phi_q$  in the  $JQ_3$  model, because of the excessive computational efforts required in order to collect sufficient data for proper analysis.

We next develop a scaling theory to understand the dynamic scaling of  $\phi_q$  more formally. By generalizing the scaling form in Ref. [48] to the non-equilibrium case, we find that the full scaling form of  $\phi_q$  should be

$$\phi_q(g, v, L) = L^{-|y_q|} f(gL^{1/\nu}, gL^{1/\nu'}; vL^r, vL^{r'}), \quad (\text{A4})$$

in which  $g \equiv T - T_c$ . For a process stopping at the critical point,  $g = 0$ , Eq. (A4) reduces to

$$\phi_q(g, v, L) = L^{-|y_q|} f(vL^r, vL^{r'}). \quad (\text{A5})$$

Since the function  $f$  should be analytic for small values of its arguments and  $r > r'$ , the argument  $vL^r$  will dominate when  $vL^{r'} \ll vL^r$ . For small velocities, Eq. (A5) can therefore be approximated as

$$\phi_q(g, v, L) = L^{-|y_q|} j(vL^r), \quad (\text{A6})$$

in which  $j$  is another scaling function. Equation (A6) explains the scaling behavior found in Fig A4(d) for the smallest values of  $v$  available for each system size.

For larger  $v$ , the scaling argument  $vL^{r'}$  must also be included, and when  $vL^r$  also becomes very large ( $vL^r \gg vL^{r'}$ ) the function  $f$  should develop a power-law in it, resulting in the form

$$\phi_q(g, v, L) = L^{-|y_q|} (vL^r)^a k(vL^{r'}), \quad (\text{A7})$$

with yet another scaling function  $k$  and with the exponent  $a$  to be determined. The above form should hold for any value of  $vL^{r'}$  as long as  $vL^r$  is large and its power law has developed. When  $\phi_q$  is close to 1 (because of the initial condition), as demonstrated in Figs. A4(b) and A4(c), Eq. (A7) should cross over to an explicitly dimensionless form;

$$\phi_q(g, v, L) = p(vL^{r'}). \quad (\text{A8})$$

Equations (A7) and (A8) now dictate that  $k(vL^{r'})$  must satisfy

$$k(vL^{r'}) = (vL^{r'})^b w(vL^{r'}) \quad (\text{A9})$$

for some function  $w(x)$  that approaches a constant for  $x \rightarrow 0$ . Combination of this scaling forms with Eq. (A7) gives that  $b = -a$ , in order to eliminate  $v$  in front of the scaling function when  $v \rightarrow 0$ , and then to eliminate  $L$  from Eq. (A7) we must have

$$a = \frac{|y_q|}{r - r'} = \frac{|y_q|}{1/\nu - 1/\nu'}. \quad (\text{A10})$$

By using the values  $\nu = 0.6717$ ,  $\nu' = 1.52$ , and  $y_6 = -2.55$  in Eq. (A10), one finds that  $a \approx 3.07$  for the  $Z_6$  model.

We can test the above chain of arguments by using the predicted value of  $a$  in Eq. (A7). As shown in Fig. A5, rescaling  $v$  and  $\phi_q$  as  $vL^{r'}$  and  $\phi_q L^{|y_q|} (vL^r)^{-a}$ , respectively, the rescaled data collapse well for both the large- $v$  and small- $v$  regions. In addition, the slope of the common curve in Fig. A5 is fully consistent with  $-3.07$ , indicating that the leading term in  $k(vL^{r'})$  in Eq. (A9) is  $(vL^{r'})^b$  with  $b = -a \approx -3.07$  as predicted above. In addition, when  $vL^{r'}$  is small we observe that the rescaled data begin to saturate, indicating that  $k(vL^{r'})$  in Eq. (A7) approaches a constant for small  $vL^{r'}$ . This behavior is consistent with the function  $k$  in Eq. (A6) being analytic when the argument is taken to zero.

All these results confirm our derivations and demonstrate that both  $\xi_v$  and  $\xi'_v$  control the dynamics of  $\phi_q$ ,

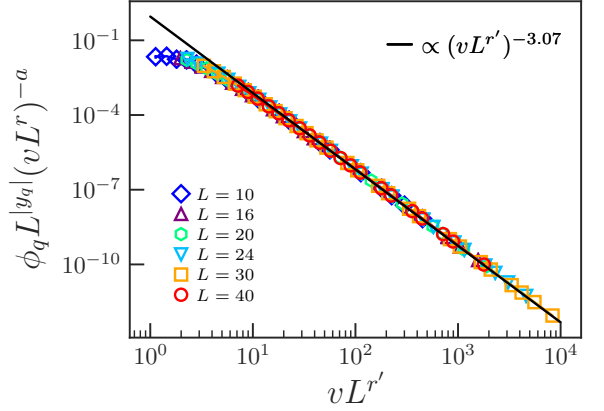


FIG. A5. **Verification of the scaling theory for  $\phi_q$ .** After rescaling  $v$  and  $\phi_q$  as  $vL^{r'}$  and  $\phi_q L^{|y_q|} (vL^r)^{-a}$  with the predicted exponent  $a = 3.07$  and with the other exponents set to their known values for the  $q = 6$  clock model, the  $\phi_q$  data for different system sizes and velocities, confirming Eq. (A7) with the derived value of  $a$ . Thus, the dynamics of  $\phi_q$  is controlled by both  $\xi_v$  and  $\xi'_v$ . The solid line indicates the power law  $(vL^{r'})^{-a}$  with the predicted exponent  $a = 3.07$ .

i.e., that the driven dynamics in the  $Z_q$ -symmetric clock model is beyond the conventional KZS mechanism. We point out that the data graphed as in Figs. A4(c) and (d) represent limiting behaviors, while the scaling function  $k$  obtained from the data collapse Fig. A5 represent the complete behavior together with Eq. (A7) and the expression for the exponent  $a$  in Eq. (A10).

In Fig. 4 in the main text, we demonstrated that the order parameter  $M^2$  is always controlled by  $\xi_v$  for driven dynamics from both the ordered phase and the disordered phase. There is a velocity regime in which  $M^2 \propto v^{2\beta/\nu r}$ , as shown in Fig. 4(a), and the scaling collapse in Figs. 4(b) and 4(c) show that the dimensionless variables in the scaling function  $f_M$  are  $vL^r$  and  $gL^{1/\nu}$ . These results demonstrate that the evolution of  $M^2$  from the ordered initial phase satisfies Eq. (A2). In addition, after annealing from a disordered initial state, Fig. 4(d) shows that  $M^2$  satisfies  $M^2 L^3 \propto v^{(2\beta - d\nu)/\nu r}$  until the cross-over to the equilibrium behavior. Again, Figs. 4(e) and 4(f) show that  $v$  and  $g$  should be rescaled as  $vL^r$  and  $gL^{1/\nu}$ , respectively. Thus, the evolution of  $M^2$  obeys conventional KZS for both annealing directions and is not affected by the presence of the longer length scale.

The driven dynamics of the  $Z_q$ -clock model has been realized in experiments as reported in Ref. [33]. There, the scaling of the defect density was shown to obey the conventional KZS, as the behavior of the order parameter  $M^2$  shown here. According to our present analyses, it would be quite instructive to further explore the driven dynamics of the angular order parameter  $\phi_q$  in this system.



- 
- [1] Senthil, T., Vishwanath, A., Balents, L., Sachdev, S. & Fisher, M. P. A. Deconfined Quantum Critical Points. *Science* **303**, 1490–1494 (2004).
- [2] Levin, M. & Senthil, T. Deconfined quantum criticality and Néel order via dimer disorder. *Phys. Rev. B* **70**, 220403 (2004).
- [3] Senthil, T. & Fisher, M. P. A. Competing orders, non-linear sigma models, and topological terms in quantum magnets. *Phys. Rev. B* **74**, 064405 (2006).
- [4] Sandvik, A. W. Evidence for Deconfined Quantum Criticality in a Two-Dimensional Heisenberg Model with Four-Spin Interactions. *Phys. Rev. Lett.* **98**, 227202 (2007).
- [5] Melko, R. G. & Kaul, R. K. Scaling in the Fan of an Unconventional Quantum Critical Point. *Phys. Rev. Lett.* **100**, 017203 (2008).
- [6] Lou, J., Sandvik, A. W. & Kawashima, N. Antiferromagnetic to valence-bond-solid transitions in two-dimensional  $SU(N)$  Heisenberg models with multispin interactions. *Phys. Rev. B* **80**, 180414 (2009).
- [7] Chen, K. *et al.* Deconfined Criticality Flow in the Heisenberg Model with Ring-Exchange Interactions. *Phys. Rev. Lett.* **110**, 185701 (2013).
- [8] Harada, K. *et al.* Possibility of deconfined criticality in  $SU(N)$  Heisenberg models at small  $N$ . *Phys. Rev. B* **88**, 220408 (2013).
- [9] Nahum, A., Chalker, J. T., Serna, P., Ortuño, M. & Somoza, A. M. Deconfined Quantum Criticality, Scaling Violations, and Classical Loop Models. *Phys. Rev. X* **5**, 041048 (2015).
- [10] Nahum, A., Serna, P., Chalker, J. T., Ortuño, M. & Somoza, A. M. Emergent  $SO(5)$  Symmetry at the Néel to Valence-Bond-Solid Transition. *Phys. Rev. Lett.* **115**, 267203 (2015).
- [11] Shao, H., Guo, W. & Sandvik, A. W. Quantum criticality with two length scales. *Science* **352**, 213–216 (2016).
- [12] Ma, N. *et al.* Dynamical signature of fractionalization at a deconfined quantum critical point. *Phys. Rev. B* **98**, 174421 (2018).
- [13] Wang, C., Nahum, A., Metlitski, M. A., Xu, C. & Senthil, T. Deconfined Quantum Critical Points: Symmetries and Dualities. *Phys. Rev. X* **7**, 031051 (2017).
- [14] Ihrig, B., Zerf, N., Marquard, P., Herbut, I. F. & Scherer, M. M. Abelian Higgs model at four loops, fixed-point collision, and deconfined criticality. *Phys. Rev. B* **100**, 134507 (2019).
- [15] Zhao, B., Takahashi, J. & Sandvik, A. W. Multicritical Deconfined Quantum Criticality and Lifshitz Point of a Helical Valence-Bond Phase. *Phys. Rev. Lett.* **125**, 257204 (2020).
- [16] Ma, R. & Wang, C. Theory of deconfined pseudocriticality. *Phys. Rev. B* **102**, 020407 (2020).
- [17] Nahum, A. Note on Wess-Zumino-Witten models and quasiuniversality in  $2+1$  dimensions. *Phys. Rev. B* **102**, 201116 (2020).
- [18] He, Y.-C., Rong, J. & Su, N. Non-Wilson-Fisher kinks of  $O(N)$  numerical bootstrap: from the deconfined phase transition to a putative new family of CFTs. *SciPost Phys.* **10**, 115 (2021).
- [19] Wang, Z., Zaletel, M. P., Mong, R. S. K. & Assaad, F. F. Phases of the  $(2+1)$  Dimensional  $SO(5)$  Non-linear Sigma Model with Topological Term. *Phys. Rev. Lett.* **126**, 045701 (2021).
- [20] Lu, D.-C., Xu, C. & You, Y.-Z. Self-duality protected multicriticality in deconfined quantum phase transitions. *Phys. Rev. B* **104**, 205142 (2021).
- [21] Liao, Y. D., Pan, G., Jiang, W., Qi, Y. & Meng, Z. Y. The teaching from entanglement: 2D deconfined quantum critical points are not conformal. *arXiv: 2302.11742* (2023).
- [22] Christos, M. *et al.* A model of  $d$ -wave superconductivity, antiferromagnetism, and charge order on the square lattice. *arXiv: 2302.07885* (2023).
- [23] Takahashi, J. & Sandvik, A. W. Valence-bond solids, vestigial order, and emergent  $SO(5)$  symmetry in a two-dimensional quantum magnet. *Phys. Rev. Res.* **2**, 033459 (2020).
- [24] Tang, Y. & Sandvik, A. W. Confinement and Deconfinement of Spinons in Two Dimensions. *Phys. Rev. Lett.* **110**, 217213 (2013).
- [25] Kibble, T. W. B. Topology of cosmic domains and strings. *Journal of Physics A: Mathematical and General* **9**, 1387 (1976).
- [26] Zurek, W. H. Cosmological experiments in superfluid helium? *Nature* **317**, 505–508 (1985).
- [27] Polkovnikov, A., Sengupta, K., Silva, A. & Vengalattore, M. Colloquium: Nonequilibrium dynamics of closed interacting quantum systems. *Rev. Mod. Phys.* **83**, 863–883 (2011).
- [28] Dziarmaga, J. Dynamics of a quantum phase transition and relaxation to a steady state. *Advances in Physics* **59**, 1063–1189 (2010).
- [29] Zhong, F. & Xu, Z. Dynamic Monte Carlo renormalization group determination of critical exponents with linearly changing temperature. *Phys. Rev. B* **71**, 132402 (2005).
- [30] De Grandi, C., Polkovnikov, A. & Sandvik, A. W. Universal nonequilibrium quantum dynamics in imaginary time. *Phys. Rev. B* **84**, 224303 (2011).
- [31] Liu, C.-W., Polkovnikov, A. & Sandvik, A. W. Dynamic scaling at classical phase transitions approached through nonequilibrium quenching. *Phys. Rev. B* **89**, 054307 (2014).
- [32] Huang, Y., Yin, S., Feng, B. & Zhong, F. Kibble-Zurek mechanism and finite-time scaling. *Phys. Rev. B* **90**, 134108 (2014).
- [33] Lin, S.-Z., Wang, X., Kamiya, Y. & *et al.* Topological defects as relics of emergent continuous symmetry and Higgs condensation of disorder in ferroelectrics. *Nature Physics* **10**, 970–977 (2014).
- [34] Clark, L. W., Feng, L. & Chin, C. Universal space-time scaling symmetry in the dynamics of bosons across a quantum phase transition. *Science* **354**, 606–610 (2016).
- [35] Rysti, J. *et al.* Suppressing the Kibble-Zurek Mechanism by a Symmetry-Violating Bias. *Phys. Rev. Lett.* **127**, 115702 (2021).
- [36] Rams, M. M., Dziarmaga, J. & Zurek, W. H. Symmetry Breaking Bias and the Dynamics of a Quantum Phase Transition. *Phys. Rev. Lett.* **123**, 130603 (2019).
- [37] Keesling, A., Omran, A., Levine, H. & *et al.* Quantum Kibble-Zurek mechanism and critical dynamics on a programmable Rydberg simulator. *Nature* **568**, 207–211

- (2019).
- [38] King, A. D. *et al.* Quantum critical dynamics in a 5,000-qubit programmable spin glass. *Nature* (2023). URL <https://doi.org/10.1038/s41586-023-05867-2>.
- [39] Gong, S., Zhong, F., Huang, X. & Fan, S. Finite-time scaling via linear driving. *New Journal of Physics* **12**, 043036 (2010).
- [40] Liu, C.-W., Polkovnikov, A., Sandvik, A. W. & Young, A. P. Universal dynamic scaling in three-dimensional Ising spin glasses. *Phys. Rev. E* **92**, 022128 (2015).
- [41] Zurek, W. H., Dorner, U. & Zoller, P. Dynamics of a Quantum Phase Transition. *Phys. Rev. Lett.* **95**, 105701 (2005).
- [42] Dziarmaga, J. Dynamics of a Quantum Phase Transition: Exact Solution of the Quantum Ising Model. *Phys. Rev. Lett.* **95**, 245701 (2005).
- [43] Polkovnikov, A. Universal adiabatic dynamics in the vicinity of a quantum critical point. *Phys. Rev. B* **72**, 161201 (2005).
- [44] Schmitt, M., Rams, M. M., Dziarmaga, J., Heyl, M. & Zurek, W. H. Quantum phase transition dynamics in the two-dimensional transverse-field Ising model. *Science Advances* **8**, eabl6850 (2022).
- [45] Shu, Y.-R., Jian, S.-K. & Yin, S. Nonequilibrium Dynamics of Deconfined Quantum Critical Point in Imaginary Time. *Phys. Rev. Lett.* **128**, 020601 (2022).
- [46] D’Emidio, J., Eberharter, A. A. & Läuchli, A. M. Diagnosing weakly first-order phase transitions by coupling to order parameters. *arXiv: 2106.15462* (2021).
- [47] Sandvik, A. W. & Zhao, B. Consistent Scaling Exponents at the Deconfined Quantum-Critical Point. *Chinese Physics Letters* **37**, 057502 (2020).
- [48] Shao, H., Guo, W. & Sandvik, A. W. Monte Carlo Renormalization Flows in the Space of Relevant and Irrelevant Operators: Application to Three-Dimensional Clock Models. *Phys. Rev. Lett.* **124**, 080602 (2020).
- [49] Oshikawa, M. Ordered phase and scaling in  $Z_n$  models and the three-state antiferromagnetic Potts model in three dimensions. *Phys. Rev. B* **61**, 3430–3434 (2000).
- [50] De Grandi, C., Polkovnikov, A. & Sandvik, A. W. Microscopic theory of non-adiabatic response in real and imaginary time. *Journal of Physics: Condensed Matter* **25**, 404216 (2013).
- [51] Liu, C.-W., Polkovnikov, A. & Sandvik, A. W. Quasi-adiabatic quantum Monte Carlo algorithm for quantum evolution in imaginary time. *Phys. Rev. B* **87**, 174302 (2013).
- [52] Sandvik, A. W. Computational Studies of Quantum Spin Systems. *AIP Conference Proceedings* **1297**, 135–338 (2010).
- [53] Tang, Y. & Sandvik, A. W. Method to Characterize Spinons as Emergent Elementary Particles. *Phys. Rev. Lett.* **107**, 157201 (2011).
- [54] Beach, K. & Sandvik, A. W. Some formal results for the valence bond basis. *Nuclear Physics B* **750**, 142–178 (2006).
- [55] Suzuki, M. Relationship between d-Dimensional Quantum Spin Systems and (d+1)-Dimensional Ising Systems: Equivalence, Critical Exponents and Systematic Approximations of the Partition Function and Spin Correlations. *Prog. Theor. Phys.* **56**, 1454 (1976).
- [56] Sachdev, S. *Quantum Phase Transitions* (Cambridge University Press, 1999).
- [57] Sondhi, S. L., Girvin, S. M., Carini, J. P. & Shahar, D. Continuous quantum phase transitions. *Rev. Mod. Phys.* **69**, 315–333 (1997).
- [58] Vojta, M. Quantum phase transitions. *Rep. Prog. Phys.* **66**, 2069 (2003).
- [59] Shu, Y.-R., Yin, S. & Yao, D.-X. Universal short-time quantum critical dynamics of finite-size systems. *Phys. Rev. B* **96**, 094304 (2017).
- [60] Hasenbusch, M. Finite size scaling study of lattice models in the three-dimensional Ising universality class. *Phys. Rev. B* **82**, 174433 (2010).
- [61] Zhong, F. Finite-time Scaling and its Applications to Continuous Phase Transitions. In Mordechai, S. (ed.) *Applications of Monte Carlo Method in Science and Engineering*, chap. 18 (IntechOpen, Rijeka, 2011).
- [62] José, J. V., Kadanoff, L. P., Kirkpatrick, S. & Nelson, D. R. Renormalization, vortices, and symmetry-breaking perturbations in the two-dimensional planar model. *Phys. Rev. B* **16**, 1217–1241 (1977).
- [63] Pujari, S., Alet, F. & Damle, K. Transitions to valence-bond solid order in a honeycomb lattice antiferromagnet. *Phys. Rev. B* **91**, 104411 (2015).
- [64] Campostrini, M., Hasenbusch, M., Pelissetto, A., Rossi, P. & Vicari, E. Critical behavior of the three-dimensional XY universality class. *Phys. Rev. B* **63**, 214503 (2001).
- [65] Lou, J., Sandvik, A. W. & Balents, L. Emergence of U(1) Symmetry in the 3D XY Model with  $Z_q$  Anisotropy. *Phys. Rev. Lett.* **99**, 207203 (2007).
- [66] Okubo, T., Oshikawa, K., Watanabe, H. & Kawashima, N. Scaling relation for dangerously irrelevant symmetry-breaking fields. *Phys. Rev. B* **91**, 174417 (2015).
- [67] Léonard, F. & Delamotte, B. Critical Exponents Can Be Different on the Two Sides of a Transition: A Generic Mechanism. *Phys. Rev. Lett.* **115**, 200601 (2015).
- [68] Hove, J. & Sudbø, A. Criticality versus  $q$  in the  $(2+1)$ -dimensional  $Z_q$  clock model. *Phys. Rev. E* **68**, 046107 (2003).
- [69] Hasenbusch, M. & Vicari, E. Anisotropic perturbations in three-dimensional  $O(N)$ -symmetric vector models. *Phys. Rev. B* **84**, 125136 (2011).
- [70] Patil, P., Shao, H. & Sandvik, A. W. Unconventional U(1) to  $Z_q$  crossover in quantum and classical  $q$ -state clock models. *Phys. Rev. B* **103**, 054418 (2021).
- [71] Chlebicki, A., Sánchez-Villalobos, C. A., Jakubczyk, P. & Wschebor, N.  $Z_4$ -symmetric perturbations to the XY model from functional renormalization. *Phys. Rev. E* **106**, 064135 (2022).
- [72] Ueno, Y. & Mitsubo, K. Incompletely ordered phase in the three-dimensional six-state clock model: Evidence for an absence of ordered phases of XY character. *Phys. Rev. B* **43**, 8654–8657 (1991).
- [73] Chubukov, A. V., Sachdev, S. & Ye, J. Theory of two-dimensional quantum Heisenberg antiferromagnets with a nearly critical ground state. *Phys. Rev. B* **49**, 11919–11961 (1994).
- [74] Miyashita, S. Nature of the Ordered Phase and the Critical Properties of the Three Dimensional Six-State Clock Model. *Journal of the Physical Society of Japan* **66**, 3411–3420 (1997).
- [75] Zhitomirsky, M. E., Holdsworth, P. C. W. & Moessner, R. Nature of finite-temperature transition in anisotropic pyrochlore  $\text{Er}_2\text{Ti}_2\text{O}_7$ . *Phys. Rev. B* **89**, 140403 (2014).
- [76] Banerjee, D., Chandrasekharan, S. & Orlando, D. Conformal dimensions via large charge expansion. *Phys. Rev. Lett.* **120**, 061603 (2018).

- [77] Hasenbusch, M. Monte Carlo study of an improved clock model in three dimensions. *Phys. Rev. B* **100**, 224517 (2019).
- [78] Jensen, L. M., Kim, B. J. & Minnhagen, P. Dynamic critical behaviors of three-dimensional XY models related to superconductors/superfluids. *Europhysics Letters* **49**, 644 (2000).